Kent Academic Repository

Martin, Richard A., Mountjoy, Gavin and Newport, Robert J. (2009) *A molecular dynamics model of the atomic structure of dysprosium alumino-phosphate glass.* Journal of Physics: Condensed Matter, 21 (7). ISSN 0953-8984.

A molecular dynamics model of the atomic structure of dysprosium alumino-phosphate glass

Richard A Martin[1], Gavin Mountjoy and Robert J Newport

School of Physical Sciences, University of Kent, Canterbury, Kent CT2 7NH, UK

E-mail: R.A.Martin@Kent.ac.uk

Abstract
Molecular dynamics (MD) has been used to identify the relative distribution of dysprosium in the phosphate glass $DyAl_{0.30}P_{3.05}O_{9.62}$. The MD model has been compared directly with experimental data obtained from neutron diffraction to enable a detailed comparison beyond the total structure factor level. The MD simulation gives $Dy \cdots Dy$ correlations at 3.80(5) and 6.40(5) Å with relative coordination numbers of 0.8(1) and 7.3(5), thus providing evidence of minority rare-earth clustering within these glasses. The nearest neighbour Dy–O peak occurs at 2.30 Å with each Dy atom having on average 5.8 nearest neighbour oxygen atoms. The MD simulation is consistent with the phosphate network model based on interlinked PO_4 tetrahedra where the addition of network modifiers Dy^{3+} depolymerizes the phosphate network through the breakage of P–(O)–P bonds whilst leaving the tetrahedral units intact. The role of aluminium within the network has been taken into explicit account, and Al is found to be predominantly (78%) tetrahedrally coordinated. In fact all four Al bonds are found to be to P (via an oxygen atom) with negligible amounts of Al–O–Dy bonds present. This provides an important insight into the role of Al additives in improving the mechanical properties of these glasses.

(Some figures in this article are in colour only in the electronic version)

1. Introduction

Rare-earth phosphate glasses are of great interest due to their many important magneto-optical [1] and opto-electronic properties [2] and their widespread application as lasing media [3]. The macroscopic properties of these materials, such as the high luminescence and long fluorescence lifetimes essential for lasing, are highly dependent upon the local environment and interactions of the rare-earth ions. Understanding and controlling these properties is reliant upon detailed structural information on the relative distribution of rare-earth ions and the local environment of the surrounding host. Consequently, there is considerable interest in the local structure of rare-earth phosphate glasses [4–30]. However, due to the structural complexity of these glasses and their numerous overlapping correlation functions it is exceptionally difficult

to measure and interpret experimental data unambiguously. Conventional x-ray and neutron diffraction techniques only provide a single measurement of the total structure factor, $F(Q)$, given by

$$F(Q) = \sum_{\alpha} \sum_{\beta} c_{\alpha} c_{\beta} b_{\alpha} b_{\beta} [S_{\alpha\beta}(Q) - 1] \qquad (1)$$

where c_{α} and b_{α} denote the atomic fraction and coherent scattering length for element α, $S_{\alpha\beta}(Q)$ is the partial structure factor and Q is the magnitude of the scattering vector. These functions of Q are referred to as reciprocal space data. The corresponding real-space data is obtained by Fourier transforming the reciprocal space data. The real-space neutron diffraction data takes the same form as equation (1), where the total pair correlation function, $G(r)$, is obtained by replacing $S_{\alpha\beta}(Q)$ with the partial pair distribution functions $g_{\alpha\beta}(r)$. A rare-earth phosphate glass containing Al, to improve mechanical properties and

---

[1] Author to whom any correspondence should be addressed.

Table 1. Relative contributions of each $S_{\alpha\beta}(Q)$ to the total structure factors and difference functions.

	$S_{DyDy}(Q)$	$S_{DyP}(Q)$	$S_{DyO}(Q)$	$S_{RAl}(Q)$	$S_{PP}(Q)$	$S_{PO}(Q)$	$S_{PAl}(Q)$	$S_{OO}(Q)$	$S_{AlO}(Q)$	$S_{AlAl}(Q)$
$^{Dy}F(Q)$	3.3	6.4	22.8	0.4	3.1	22.3	0.4	39.8	1.5	0.01
$\Delta_{Dy\mu}(Q)$	0	21.6	77.0	1.4	0	0	0	0	0	0
$\Delta_{\mu\mu'}(Q)$	0	0	0	0	4.6	33.2	0.6	59.3	2.2	0.01
$S_{DyDy}(Q)$	100	0	0	0	0	0	0	0	0	0

enable optical fibres to be drawn [31], contains four elements and is therefore described by ten overlapping pair functions $S_{\alpha\beta}(Q)$ or $g_{\alpha\beta}(r)$. Consequently, individual pairwise correlations in $G(r)$ cannot be unambiguously separated and real-space correlations can only be identified to ∼3 Å, after which pairwise correlation functions will increasingly tend to overlap. Indeed, it is only within the last five years that detailed experimental information on the rare-earth environment and distribution has been provided by employing a range of challenging neutron diffraction experiments including isomorphic substitution [17, 18], anomalous dispersion [25, 26] and a magnetic difference neutron diffraction method [23]. The lack of detailed experimental information for comparison with and validation of computer simulations has severely hampered progress in this field; to date there has only been one reported molecular dynamics model of a rare-earth phosphate glass [24].

The present work uses MD simulations to model the structure of a dysprosium alumino-phosphate glass, $DyAl_{0.30}P_{3.05}O_{9.62}$. The composition has been selected due to the large amount of experimental information [17, 18] readily available to compare with and validate the MD model. Generally, MD models are validated by comparing a single MD model with a single total diffraction pattern. However, even when there is good overall agreement between the MD model and total correlations from experimental data it is not usually possible separately to compare selected correlations between MD models and experiment. The experimental work, which employed the method of isomorphic substitution, enabled selected correlations such as the *rare-earth–matrix* terms (matrix = P, O and Al), the *matrix–matrix* terms and the *rare-earth–rare-earth* correlation to be deconvolved from the total structure factor. This detailed experimental data allows a much more rigorous validation of the model and comparison with experimental data beyond the total structure factor level. Full details on the method of isomorphic substitution in neutron diffraction are given by Martin *et al* [17, 18]. In essence the technique relies upon measuring samples that may reasonably be regarded as structurally identical and which differ only in their coherent neutron scattering length. Total structure factors with different scattering lengths are then combined to eliminate selected correlations and thereby reduce the effective complexity of the system. In the experimental work Dy^{3+} and Ho^{3+} were selected since they have comparable ionic radii [32] and Pettifor chemical parameters [33], and share a similar structural chemistry [34].

For the particular dysprosium alumino-phosphate glass of interest in the present study, which contains ten partial structure factors, it is clearly evident that the large number of individual overlapping correlations cannot be justified by

a single agreement between experimentally derived data and a MD model. The total diffraction pattern for $DyAl_{0.30}P_{3.05}O_{9.62}$, is dominated by the P–O and O$\cdots$O correlations and thus one may argue that a comparison between total structure factors provides little more than an insight into the host phosphate network. It is, however, the weaker and/or obscured R–O and R$\cdots$R correlations that are of greatest significance. The relative contributions to the total structure factor is given in table 1; the P–O and O$\cdots$O correlations account for 62% of the total structure factor whilst the Dy–O, Dy$\cdots$P and Dy$\cdots$Dy correlation account for only 23%, 6% and 3% respectively. Isolating the Dy-*matrix* terms to form a function containing only Dy–O, Dy$\cdots$P and Dy$\cdots$Al correlations increases the relative Dy–O contribution to 77% and the Dy$\cdots$P correlation to 22%. By definition the *rare-earth–rare-earth* term contains 100% Dy$\cdots$Dy correlations. These difference functions therefore enable much more rigorous comparisons of the molecular dynamic model with experimental data for the Dy–O and Dy$\cdots$Dy correlations.

This study presents only the second ever MD model of a rare-earth phosphate glass and is the first MD simulation to include aluminium ions, thus increasing the complexity from three to four elements. The number of atoms in the model has also been doubled compared to the earlier study [24] to compensate for the low concentration of Al and to reduce the edge effects of the simulation box.

2. Molecular dynamics method

P–O, Dy–O, Al–O and O$\cdots$O interactions were described using rigid ion potentials, as this allows the large number of time-steps necessary for modelling glasses. The parameters were taken from those derived by Teter [36], which have proven effective for modelling phosphate [24], silicate [37] and aluminate [38] glasses. The potentials have the form

$$V_{\alpha\beta}(r) = \frac{q_\alpha q_\beta}{4\pi\varepsilon_0 r} + A_{\alpha\beta}\exp\left(\frac{-r}{\rho_{\alpha\beta}}\right) - \frac{C_{\alpha\beta}}{r^6} \qquad (2)$$

where $V_{\alpha\beta}(r)$ is the potential, α and β are element types, r is inter-atomic distance, q is the effective charge, and $A_{\alpha\beta}$, $\rho_{\alpha\beta}$ and $C_{\alpha\beta}$ are potential parameters (with $\varepsilon_0 = 8.854 \times 10^{-12}$ C^2 N^{-1} m^{-2}). The potential parameters are shown in table 2. In addition, potential parameters for O–P–O and P–O–P bond bending interactions were taken from [24], and have the form

$$V_{\alpha\beta\alpha}(\theta) = \tfrac{1}{2}k_{\alpha\beta\alpha}(\theta - \Theta_{\alpha\beta\alpha})^2 \qquad (3)$$

where β is the element type of the central atom, $k_{\alpha\beta\alpha} = 3.5$ eV and $\Theta_{\alpha\beta\alpha} = 109.47°$ for O–P–O, and $k_{\alpha\beta\alpha} = 3.0$ eV and $\Theta_{\alpha\beta\alpha} = 135.5°$ for P–O–P.

Table 2. Two-body potential parameters used in this study [36].

α–β	q_α (e)	$A_{\alpha\beta}$ (eV)	$\rho_{\alpha\beta}$ (Å)	$C_{\alpha\beta}$ (eV Å^{-6})
P–O	3.0	27 722	0.1819	86.86
Dy–O	1.8	79 812	0.1947	62.51
Al–O	1.8	12 201	0.1956	31.99
O$\cdots$O	−1.2	1 844	0.3436	192.58

MD was used to obtain a model of the atomic structure of glassy $DyAl_{0.3}P_{3.05}O_{9.62}$ in order to compare with the detailed experimental neutron diffraction results from the same glass [17, 18]. The model has a total of 2600 atoms (186 Dy, 56 Al, 570 P and 1788 O) in a cubic box with a length of 33.1 Å, the box size corresponds to a number density of 0.0715 atoms Å^{-3}, as determined experimentally [17, 18]. A random starting configuration and periodic boundary conditions were used. MD modelling used the DLPOLY program [39] with time-steps of 1 fs. A Berendsen NVT algorithm was used with a relaxation time of 2 ps. A short range cut-off of 10 Å was used for all except the Coulomb potential, and the Coulomb potential was calculated using the Ewald method with a precision of 10^{-5}. The modelling used six stages. The first three stages were temperature baths of 80 000 time-steps (with equilibration) at 6000, 3000, and 1500 K. (A trajectory of 80 000 time-steps at 6000 K is sufficient to allow diffusion over the box length. During the first three stages the simulation box size is expanded by factors of 1.03, 1.015 and 1.005 respectively to allow for thermal expansion.) The fourth stage was a temperature quench of 60 000 time-steps (with equilibration) from 1500 to 300 K, i.e. a quench rate of 10^{13} K s^{-1}. Due to constraints on computing time, all MD studies of glasses use quench rates that are several orders of magnitude higher than in experiments. However this quench rate is typical in MD studies of glasses, e.g. in [24, 37–39]. The final two stages were temperature baths of 80 000 time-steps at 300 K (the first with equilibration and the second without equilibration). During the final stage, structural parameters were sampled (every 200 time-steps) to include disorder due to thermal vibrations, which is present in the experimental results.

3. Results

Figure 1 shows an image of the MD model of $DyAl_{0.3}P_{3.05}O_{9.62}$ glass, the tetrahedral PO_4 network is clearly evident. Figure 2 shows selected partial radial distribution functions $T_{\alpha\beta}(r)$ obtained from the MD model, where $T_{\alpha\beta}(r) = 4\pi r\rho g_{\alpha\beta}(r)$ and ρ is the atomic number density. The real-space correlations are described in terms of average separation, $r_{\alpha\beta}$, and the mean coordination number of β around α is denoted by $\bar{n}_\alpha^\beta$. The first peak in $T_{PO}(r)$ at ∼1.5 Å represents P–O nearest neighbours. The oxygen atoms have either two bonds to P and form part of the tetrahedral network, these oxygen atoms being called bridging oxygen (denoted O_B), or have one bond to P and therefore take no part in the tetrahedral network, these oxygen atoms being called terminal oxygen (denoted O_T) (these are also sometimes referred to as non-bridging oxygen atoms). The MD model gives 29% of O_B and 71% of O_T. According to
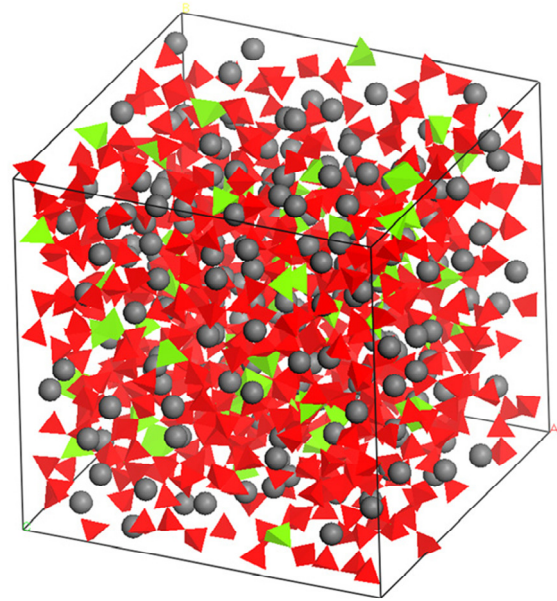

Figure 1. (Colour online) Image of the $DyAl_{0.3}P_{3.05}O_{9.62}$ model. Dark tetrahedra (red online) represent the phosphate network, the light tetrahedral (green online) represent the Al and the grey spheres represent the Dy^{3+} atoms.
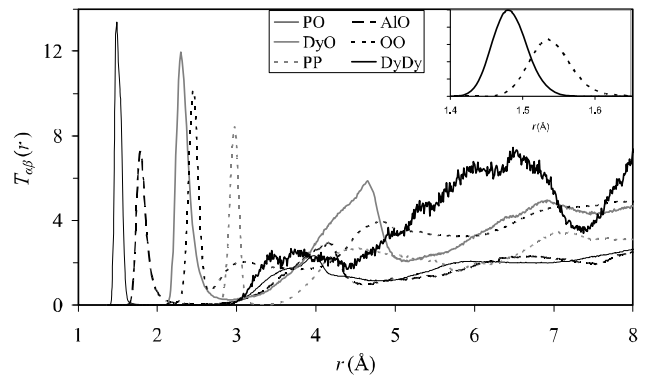

Figure 2. Selected real-space correlations obtained from the MD model. Left to right, P–O, Al–O, Dy–O, O$\cdots$O, P$\cdots$P and Dy$\cdots$Dy are given. Note that P–O, Al–O and Dy$\cdots$Dy have been scaled by 0.5, 0.5 and 15, respectively, and Dy$\cdots$P, Dy$\cdots$Al, P$\cdots$Al and Al$\cdots$Al correlations have been omitted for clarity. The inset shows the PO_T (solid curve) and PO_B (broken curve) bonds.

the phosphate model the addition of network modifiers such as Dy_2O_3 or Al_2O_3 depolymerizes the phosphate network through the breakage of P–O_B–P bonds into PO_T bonds whilst leaving the PO_4 tetrahedra intact. Specifically, if y oxygen atoms from the network modifier are added per P_2O_5 unit, the P:O_B:O_T ratio changes from 2:3:2 in pure P_2O_5 to 2:(3 − y):2(1 + y) in the modifier. On the basis of the phosphate model 27% O_B and 73% O_T are expected. The inset of figure 2 shows that P–O_T bonds are shorter than P–O_B bonds, as expected. In the model, these bonds differ by 0.06(1) Å. The P–O splitting could not be resolved experimentally but was estimated to be ∼0.10(1) Å [17, 18].

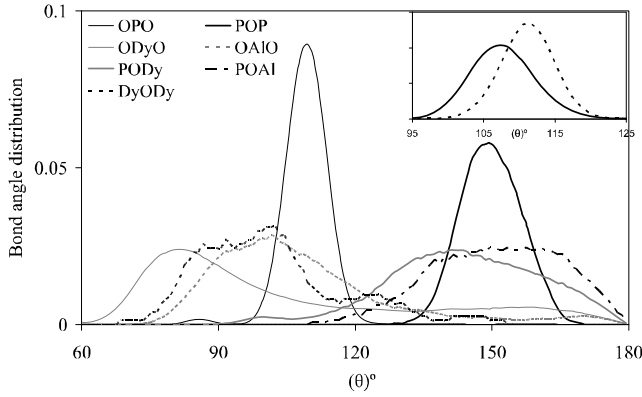The model has 98.6% P with four-fold coordination. The remaining 1.4% of P have five-fold coordination, and this

Figure 3. Bond angle distribution for DyAl$_{0.3}$P$_{3.05}$O$_{9.62}$ glass. The inset shows the O$_B$–P–O$_B$ (solid curve) and O$_T$–P–O$_T$ (broken curve) bond angles.

should be considered as a defect arising from slight inaccuracy in the potentials. This compares with 3.6% of five-fold P reported in the TbP$_3$O$_9$ MD simulation [24], this reduction in defects suggests the Dy–O potential parameters are slightly better defined than the Tb–O potentials. $T_{OO}(r)$ has a first peak at 2.5 Å due to O–P–O configurations (a very small feature at 2.2 Å occurs due to five-fold coordinated P defects). Figure 3 shows that the average O–P–O bond angle is tetrahedral, i.e. 109° (a very small feature at 85° occurs due to five-fold coordinated P defects). The inset of figure 3 shows that O$_T$–P–O$_T$ bond angles are expanded, and O$_B$–P–O$_B$ bond angles are contracted. This is expected, since O$_T \cdots$ O$_T$ neighbours experience greater repulsion than O$_B \cdots$ O$_B$ neighbours.

$T_{PP}(r)$ has a narrow first peak at $\sim$3.0 Å representing P $\cdots$ P nearest neighbours in the phosphate network, and figure 3 shows that P–O–P bond angles are peaked at around 150°. The connectivity of the phosphate network can be described by the Q^n distribution (each P is classified as Q^n, where n is equal to the number of O$_B$), and there is a majority of Q^2 groups (42%) but also significant amounts of Q^1 (32%) and Q^3 (18%) groups, with an average of $n = 1.8$ (the remainder of Q^n groups are Q^0 (6%) and Q^4). This average n is slightly high compared to the expected average of $n = 1.7$ for the modelled composition due to five-fold coordinated P defects.

The first peak in $T_{AlO}(r)$ at 1.8 Å represents Al–O nearest neighbours. The majority of Al has four-fold coordination (79%) with the remaining five-fold coordination (20%) and six-fold (1%), giving an average $\bar{n}^O_{Al} = 4.2$. All Al is bonded only to O$_T$. The first peak in $T_{DyO}(r)$ at 2.3 Å represents Dy–O nearest neighbours. The majority of Dy has five-fold (29%) and six-fold coordination (62%), with the remaining Dy (9%) having seven-fold coordination, giving an average $\bar{n}^O_{Dy} = 5.8$. All Dy is bonded only to O$_T$. $T_{OO}(r)$ has a broad second peak from 2.8 to 3.5 Å representing O$_T$ coordinated to Al and Dy, i.e. O$_T$–Al–O$_T$ and O$_T$–Dy–O$_T$ configurations, where Dy dominates due to its higher concentration. The O$_T$–Al–O$_T$ bond angle shown in figure 3 represents AlO$_T$ polyhedra, and is centred at $\sim$100°, due to the influence of some five coordinated Al. The O$_T$–Dy–O$_T$ bond angle shown in figure 3 represents

DyO$_T$ polyhedra, and is peaked at $\sim$80° with a shoulder at larger angles extending to 180°, as expected for distorted octahedral coordination. The first peak in $T_{AlP}(r)$ at 3.2 Å represents Al $\cdots$ P nearest neighbours and $\bar{n}^P_{Al} = 4.2$. Since $\bar{n}^P_{Al} = \bar{n}^O_{Al} = 4.2$ it is evident that each oxygen atom connected to an aluminium atom is also connect to a phosphorus atom; note this is in contrast to phosphorus atoms which on average have slightly less than half of the oxygen atoms connected to a second phosphorus atom. The Al is therefore found to enter the network in a tetrahedral environment, as does phosphorus, but Al has a Q^n speciation of 4, which is much higher than the Q^n speciation of phosphorus.

The first peak in $T_{PDy}(r)$ at $\sim$3.7 Å represents P $\cdots$ Dy nearest neighbours with $\bar{n}^{Dy}_P = 1.7$. The main feature in $T_{AlDy}(r)$ is at $\sim$5.5 Å with a small peak at $\sim$3.5 Å. The small number of $\bar{n}^{Dy}_{Al} \sim 0.4$ at 3.5 Å infers that Dy does not preferentially bond with oxygen atoms connected to aluminium atoms. This is consistent with all Al preferentially bonding via oxygen to phosphorus with no additional Al available to bond with Dy. Again this shows the different behaviour of Al compared to phosphorus. The Dy $\cdots$ Dy correlations show a small peak around 3.5–4 Å followed by a larger, broad peak around 6 Å. The former arises due to sharing of O$_T$, i.e. Dy–O$_T$–Dy configurations, or corner-sharing TbO$_T$ polyhedra.

Only one set of experimental results has been reported for DyAl$_{0.3}$P$_{3.05}$O$_{9.62}$, the present model will therefore be compared in detail with these results [17, 18]. Given the isomorphic nature of these materials the MD results will also be compared, where appropriate, with other rare-earth phosphates such as yttrium and terbium which are also believed to be iso-structural. To enable a direct comparison of the MD model with experimental data the real-space correlations obtained from the MD model were Fourier transformed into reciprocal space and scaled by the weighting factors $c_\alpha b_\alpha c_\beta b_\beta$ to form the total structure factor $^{Dy}F(Q)$, see figure 4. The coherent scattering lengths are 16.02, 3.449, 5.13 and 5.803 fm for Dy, Al, P and O, respectively [17, 18, 35]. The experimental data for $^{Dy}F(Q)$ is also shown in figure 4 for comparison.

The method of isomorphic substitution employed during the experimental work also enabled certain correlations to be separated from the measured total structure factor $^{Dy}F(Q)$ (see [17, 18]). Specifically, those correlation that only involve (i) the R-matrix atom correlations, $\Delta_{R\mu}(Q)$, (ii) the matrix–matrix atom correlations, $\Delta_{\mu\mu'}(Q)$, and (iii) the R–R atom correlation, $S_{RR}(Q)$, were isolated. R represents the rare-earth ion and μ (or μ') denotes Al, P or O. The *R-matrix* atom correlations, $\Delta_{R\mu}(Q)$, is given by

$$\Delta_{R\mu}(Q) = \sum_\mu 2c_R c_\mu b_\mu \delta_R [S_{R\mu}(Q) - 1] \qquad (4)$$

where δ represents an effective coherent scattering length of the rare-earth ions, in this case $\delta_R = b_{Dy} - b_{Ho}(8.01)$. The *matrix–matrix* correlations $\Delta_{\mu\mu'}(Q)$ is given by

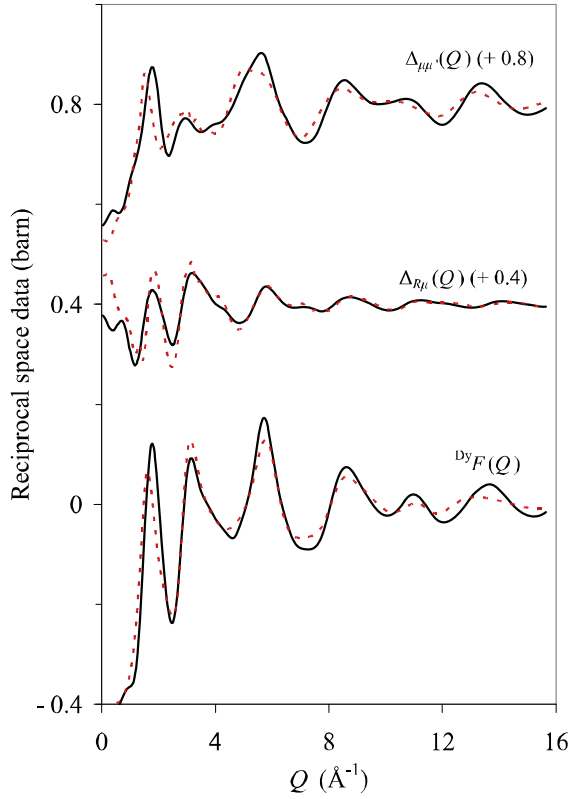$$\Delta_{\mu\mu'}(Q) = \sum_\mu \sum_{\mu'} c_\mu c_{\mu'} b_\mu b_{\mu'} [S_{\mu\mu'}(Q) - 1]. \qquad (5)$$

Figure 4. The MD reciprocal space data for $^{Dy}F(Q)$, $\Delta_{R\mu}(Q)$ and $\Delta_{\mu\mu'}(Q)$ (solid curve) and the corresponding experimental data (broken curve) [17, 18].

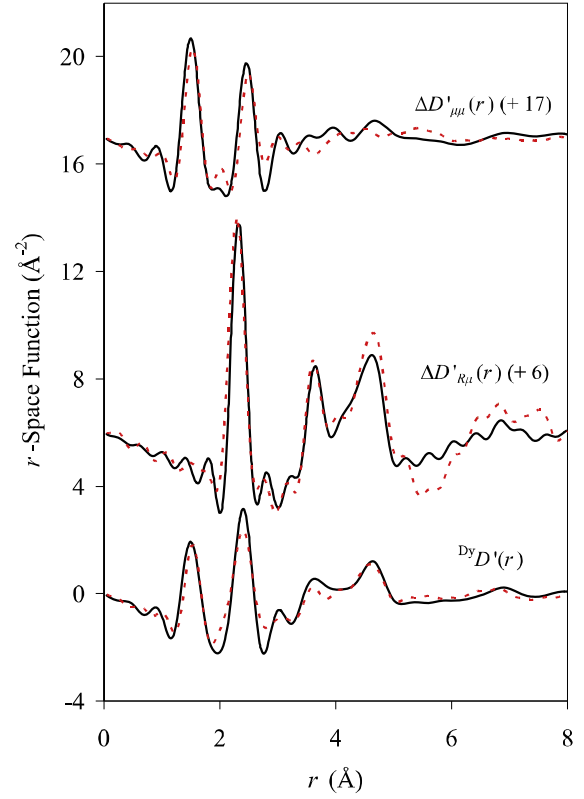**Figure 5.** The real-space functions $^{Dy}D(r)$, $\Delta D'_R(r)$ and $\Delta D'_{\mu\mu'}(r)$ obtained by Fourier transforming the corresponding reciprocal space data given in figure 4. MD model are given by the solid curve and the experimental data [17, 18] the broken curve.

Forming these difference functions separates the 10 overlapping $S_{\alpha\beta}(Q)$ correlation functions of $^{Dy}F(Q)$ to 3 for $\Delta_{R\mu}(Q)$, 6 for $\Delta_{\mu\mu'}(Q)$, and 1 for and $S_{RR}(Q)$.

The reciprocal space data $^{Dy}F(Q)$, $\Delta_{R\mu}(Q)$ and $\Delta_{\mu\mu'}(Q)$ obtained from the MD models and using equations (4), and (5) respectively are shown in figure 4 together with experimental data obtained by Martin *et al* [17, 18]. The corresponding real-space data, obtained by Fourier transforming (FT) the data in figure 4, are shown in figure 5. The MD correlations are not broadened by instrumental effects such as a limited Q range. To enable a direct comparison with experimental data the MD data was truncated at $Q_{max} = 15.65$ Å^{-1}, and a Hanning window function applied to the total structure factor, $^{Dy}F(Q)$, and the *matrix–matrix* correlation, $\Delta_{\mu\mu'}(Q)$, prior to Fourier transforming into real space.

Figures 6 and 7 show the real and reciprocal space data for $S_{DyDy}(Q)$ from the MD model together with the experimental $S_{RR}(Q)$ of Martin *et al* [17, 18] and the experimental $S_{TbTb}(Q)$ of Cole *et al* [23]. The data has been scaled to overlay, this scaling represents the difference in the coherent scattering factors used to obtain the $S_{RR}(Q)$ functions. In the present MD model $b_{Dy} = 16.02$ fm whilst the $S_{TbTb}(Q)$ function was obtained from the magnetic form factor which is not well defined and only relative values could be obtained [23], and the experimental isomorphic work uses a combination of scaled b_{coh} (Dy) and b_{coh} (Ho) [17, 18]. The MD model shows the main Dy$\cdots$Dy correlation is a broad asymmetric feature at

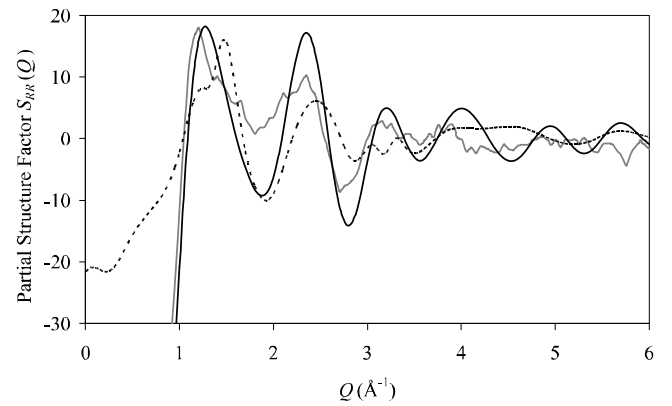**Figure 6.** The MD partial structure factor $S_{RR}(Q)$ for glassy DyAl$_{0.3}$P$_{3.05}$O$_{9.62}$ (solid dark curve), experimental $S_{RR}(Q)$ for Dy/Ho [17, 18] (broken curve) and experimental $S_{RR}(Q)$ for Tb [23] (solid grey curve).

6.30(5) Å where $\bar{n}_{Dy}^{Dy} = 7.3(5)$ a second feature at 3.80(5) Å is also evident with $\bar{n}_{Dy}^{Dy} = 0.8(1)$.

4. Discussion

The results obtained from the MD model are in good overall agreement with experimental data. The glass structure is dominated by PO$_4$ tetrahedra as shown in figure 1. The tetrahedra network is consistent with phosphate models based
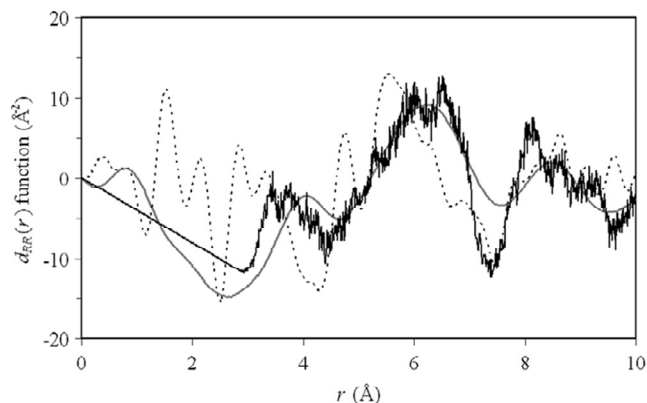
Figure 7. The real-space functions $d_{RR}(r)$ obtained by Fourier transforming the corresponding reciprocal space data given in figure 6. MD $d_{RR}(r)$ for glassy $DyAl_{0.3}P_{3.05}O_{9.62}$ (solid dark curve), experimental $d_{RR}(r)$ for Dy/Ho [17, 18] (broken curve) and experimental $d_{RR}(r)$ for Tb [23] (solid grey curve).

on interlinked PO_4 tetrahedra where the addition of rare-earth network modifiers R^{3+} depolymerize the phosphate network through the breakage of P–(O)–P bonds whilst leaving the tetrahedral units intact.

The Al–O structural parameters determined from the model, $r_{AlO} = 1.78$ Å and $\bar{n}_{Al}^O$ of 4.2, are in contrast with experimental values of $r_{AlO} = 1.89$ Å and $\bar{n}_{Al}^O$ of 5.5 obtained using isomorphic substitution which were originally reported. However, a more recent discussion of those experimental values included the statement that $\bar{n}_{Al}^O$ of 4.3 would be plausible [27]. The MD values are, however, in excellent agreement with experimental values obtained more recently, using a combination of NMR and neutron diffraction, for yttrium phosphate glasses containing small amounts aluminium where values of $r_{AlO} = 1.76(1)$ Å and $\bar{n}_{Al}^O$ of 4.2 were reported [27]. The r_{AlO} distance is also in close agreement with tetrahedral coordinated Al–O found in other glass systems [40]. Furthermore, octahedral coordinated Al with a distance $r_{AlO} = 1.88$ Å gives an O–(Al)–O nearest neighbour separation of $\sqrt{2}r_{AlO} = 2.66$ Å, whereas tetrahedral coordinated Al at a distance $r_{AlO} = 1.88$ Å gives an O–(Al)–O nearest neighbour separation of $\sqrt{8/3}r_{AlO} = 2.87$ Å; and the O···O correlation is a minimum at 2.66 Å. The large Al–O uncertainty in the initial experimental neutron diffraction data is primarily attributed to the large error associated with measuring a relatively small feature that is masked by large overlapping P–O correlations; see figure 2(c) of [18]. The P–O weighting factor ($c_Pc_Ob_Pb_O$) is over 15 times greater than the Al–O weighing factor for these glasses which, when coupled with the broadening effect of truncating Q_{max} at 15.65 Å^{-1}, makes it difficult to resolve clearly the Al–O correlation.

Al is found to enter the network in a tetrahedral environment, Al is also found to have a Q^n speciation of four where each Al–O bond is also connected to a phosphorus atom. This is consistent with the entire Al being preferentially bonding via oxygen to phosphorus with no additional Al available to bond with Dy. Al is added to the glass to improve mechanical properties and enable fibre-drawing, and it seems

reasonable to attribute these improved properties to the strong preference for Al to bond via oxygen to four phosphorus. Al links up different segments of the phosphate network with relatively strong P–O–Al–O–P connections (the tetrahedral Al–O bonds having a bond valence of ~0.75) compared to P–O–Dy–O–P connections (the six coordinated Dy–O bonds having bond valence of ~0.5). The Q^4 units formed by Al are compatible with the phosphate tetrahedral network and increase linkages while maintaining flexibility.

The nearest neighbour Dy–O peak is at 2.30 Å with $\bar{n}_{Dy}^O = 5.8(1)$. Experimentally, R–O values of $\bar{n}_R^O = 6.2(1)$ at 2.30 Å and $\bar{n}_R^O = 0.5(1)$ at 2.67 Å were obtained for the Dy, Ho isomorphic substitution [17, 18]. Although a more recent discussion of those experimental values included the statement that an overall $\bar{n}_R^O$ of 6.0 would be plausible [27]. The first R–O peak position at 2.30 Å is in agreement with experimental data. There is no evidence of the experimentally observed second R–O feature at ~2.67 Å in the MD model, although the model's R–O peak has a shoulder extending up to 3.0 Å. A second R–O peak in the region 2.5–3.5 Å is not expected on the basis of crystalline rare-earth phosphates. For c-ErP$_3$O$_9$ the shortest R–O distance is 2.17 Å and the second nearest neighbour is 3.83 Å [41]. The corresponding distances are 2.29 and 3.99 Å for c-HoP$_5$O$_{14}$ [42] and 2.31 and 4.14 Å for c-HoPO$_4$ [43]. The total R–O coordination number obtained experimentally, 6.7(1), is also significantly larger than results obtained from the MD model, 5.8. The total Dy–O coordination of 5.8 obtained from the MD model is similar to results recently reported for yttrium phosphate glasses containing small molar fractions of aluminium where a $\bar{n}_R^O = 5.75$ was obtained for neutron diffraction data with Q_{max} of 49.5 Å [27]. The MD result of $\bar{n}_{Dy}^O = 5.8$ is also in better agreement with the corresponding crystalline structure, RP$_3$O$_9$, where values of $\bar{n}_R^O = 6.0$ is obtained [41].

The MD model shows the main Dy···Dy correlation is a broad asymmetric feature at 6.30(5) Å where $\bar{n}_{Dy}^{Dy} = 7.3(5)$. A second smaller feature at 3.80(5) Å with $\bar{n}_{Dy}^{Dy} = 0.8$ is also present; this shorter distance represents Dy–O$_T$–Dy correlations and provides evidence of minority rare-earth clustering within these glasses. The MD is in good agreement with results presented by Cole *et al* [23] for a rare-earth alumino-phosphate (R = Tb, which is also believed to be iso-structural with Dy) where the main feature in the R···R correlation was at distance of 6.4 Å with a smaller feature identified at 3.9 Å. The previous MD study of Tb meta-phosphate glass showed an R···R correlation with a small peak around 3.9 Å with $\bar{n}_{Tb}^{Tb} = 0.9$ and a larger peak around 6.1 Å with $\bar{n}_{Tb}^{Tb} = 7.7$ [24]. Recent work by Hoppe using reverse Monte Carlo modelling of Er meta-phosphate glass [30] also showed an R···R correlation with main feature at 6.2 Å having $\bar{n}_R^R = 7.14$ and a second smaller feature at 4.3 Å having $\bar{n}_R^R = 0.8$.

5. Conclusions

This work presents only the second MD simulation for a rare-earth phosphate glass, the first MD simulation to include the

effect of aluminium (thereby also increasing the complexity from 6 to 10 partial structure factors) and is also the first model of a specific empirical composition instead of the nominal meta-phosphate composition (RP_3O_9). The model therefore enabled a direct comparison with experimental data without the need to allow for compositional variations.

A total of 18 potential parameters were used to model the short/intermediate range order in glassy $DyAl_{0.30}P_{3.05}O_{9.62}$. The molecular dynamic simulation was compared with detailed experimental data, including the total structure factor $^{Dy}F(Q)$, R-*matrix* function $\Delta_{R\mu}(Q)$, *matrix–matrix* correlation $\Delta_{\mu\mu'}(Q)$ and the R–R correlation $S_{RR}(Q)$ to enable a strong validation of the model. The MD model is in good overall agreement with experimental results for nearest neighbour distances and coordination numbers. The main difference was in the coordination of Al, which was the most difficult to identify experimentally, but the MD model has shown that Al preferentially adopts tetrahedral coordination, linked to four phosphorus. This simulation provides an excellent starting point from which further models can be developed for materials with lower, optical level, concentrations of R^{3+} (which cannot be measured using conventional diffraction techniques due to the small weighting factors). This will thereby enable models to be developed for realistic, dopant level, concentrations found in lasers and other optical devices.

Acknowledgment

References

[1] Carini G, D'Angelo G, Tripodo G, Fontana A, Rossi F and Saunders G A 1997 *Europhys. Lett.* **40** 435
[2] Weber M J 1991 *Materials Science and Technology* vol 9, ed J Zrzycki (Weinheim: VCH) p 654
[3] Weber M J 1990 *J. Non-Cryst. Solids* **123** 208
[4] Bowron D T, Newport R J, Rainford B D, Saunders G A and Senin H B 1995 *Phys. Rev. B* **51** 5739
[5] Bowron D T, Bushnell-Wye G, Newport R J, Rainford B D and Saunders G A 1996 *J. Phys.: Condens. Matter* **8** 3337
[6] Bowron D T, Saunders G A, Newport R J, Rainford B D and Senin H B 1996 *Phys. Rev. B* **53** 5268
[7] Hoppe U, Kranold R, Stachel D, Barz A and Hannon A C 1998 *J. Non-Cryst. Solids* **232–234** 44
[8] Anderson R, Brennan T, Cole J M, Mountjoy G, Pickup D M, Newport R J and Saunders G A 1999 *J. Mater. Res.* **14** 4706
[9] Cole J M, van Eck E R H, Mountjoy G, Newport R J, Brennan T and Saunders G A 1999 *J. Phys.: Condens. Matter* **11** 9165
[10] Shikerkar A G, Desa J A E, Krishna P S R and Chitra R 2000 *J. Non-Cryst. Solids* **270** 234
[11] Cole J M, Newport R J, Bowron D T, Pettifer R F, Mountjoy G, Brennan T and Saunders G A 2001 *J. Phys.: Condens. Matter* **13** 6659
[12] Mountjoy G, Cole J M, Brennan T, Newport R J, Saunders G A and Wallidge G W 2001 *J. Non-Cryst. Solids* **279** 20
[13] Cole J M, van Eck E R H, Mountjoy G, Anderson R, Brennan T, Bushnell-Wye G, Newport R J and Saunders G A 2001 *J. Phys.: Condens. Matter* **13** 4105
[14] Karabulut M, Metwalli E and Brow R K 2001 *J. Non-Cryst. Solids* **283** 211
[15] Karabulut M, Marasinghe G K, Metwalli E, Wittenauer A K, Brow R K, Booth C H and Shuh D K 2002 *Phys. Rev. B* **65** 104206
[16] Hoppe U, Metwalli E, Brow R K and Neuefeind J 2002 *J. Non-Cryst. Solids* **297** 263
[17] Martin R A, Salmon P S, Fischer H E and Cuello G J 2003 *Phys. Rev. Lett.* **90** 185501
[18] Martin R A, Salmon P S, Fischer H E and Cuello G J 2003 *J. Phys.: Condens. Matter* **15** 8235
[19] Martin R A, Salmon P S, Benmore C J, Fischer H E and Cuello G J 2003 *Phys. Rev. B* **68** 054203
[20] Martin R A, Salmon P S, Fischer H E and Cuello G J 2004 *J. Non-Cryst. Solids* **345/346** 208
[21] Karabulut M, Metwalli E, Wittenauer A K, Brow R K, Marasinghe G K, Booth C H, Bucher J J and Shuh D K 2005 *J. Non-Cryst. Solids* **351** 795
[22] Hoppe U, Brow R K, Ilieva D, Jovari P and Hannon A C 2005 *J. Non-Cryst. Solids* **351** 3179
[23] Cole J M, Hannon A C, Martin R A and Newport R J 2006 *Phys. Rev. B* **73** 104210
[24] Clarke E B, Mead R N and Mountjoy G 2006 *J. Phys.: Condens. Matter* **18** 6815
[25] Cole J M, Wright A C, Newport R J, Sinclair R N, Fischer H E, Cuello G J and Martin R A 2007 *J. Phys.: Condens. Matter* **19** 056002
[26] Wright A C, Cole J M, Newport R J, Fisher C E, Clarke S J, Sinclair R N, Fischer H E and Cuello G J 2007 *Nucl. Instrum. Methods Phys. Res.* A **571** 622
[27] Martin R A, Salmon P S, Carroll D L, Smith M E and Hannon A C 2007 *J. Phys.: Condens. Matter* **20** 115204
[28] Cole J M and Newport R J 2007 *J. Non-Cryst. Solids* **353** 1773
[29] Mountjoy G 2007 *J. Non-Cryst. Solids* **353** 2029
[30] Hoppe U 2008 *J. Phys.: Condens. Matter* **20** 165206
[31] Martin R A and Knight J C 2006 *IEEE Photon. Technol. Lett.* **18** 574
[32] Shannon R D 1976 *Acta Crystallogr.* A **32** 751
[33] Pettifor D G 1986 *J. Phys. C: Solid State Phys.* **19** 285
[34] Wells A F 1984 *Structural Inorganic Chemistry* 5th edn (Oxford: Clarendon)
[35] Sears V F 1992 *Neutron News* **3** 26
[36] Teter D 2004 private communication
[37] Cormack A N and Du J 2004 *J. Non-Cryst. Solids* **349** 66
[38] Thomas B W M, Mead R N and Mountjoy G 2006 *J. Phys.: Condens. Matter* **18** 1
[39] Smith W and Forester T 1996 *J. Mol. Graph.* **14** 136
[40] Hannon A C and Parker J M 2000 *J. Non-Cryst. Solids* **274** 102
[41] Dorokhova G I and Karpov O G 1984 *Sov. Phys.—Crystallogr.* **29** 400
[42] Bagieu M, Tordjman I, Durif A and Bassi G 1973 *Cryst. Struct. Commun.* **3** 387
[43] Ni Y, Hughes J M and Mariano A N 1995 *Am. Mineral.* **80** 21